Miao *et al.*
Protection and Control of Modern Power Systems (2023) 8:18
https://doi.org/10.1186/s41601-023-00292-z

Protection and Control of
Modern Power Systems

ORIGINAL RESEARCH

Open Access

A multi-energy inertia-based power support strategy with gas network constraints

Cairan Miao[1], Qi Wang[1*] and Yi Tang[1]

Abstract

An integrated energy system with multiple types of energy can support power shortages caused by the uncertainty of renewable energy. With full consideration of gas network constraints, this paper proposes a multi-energy inertia-based power support strategy. The definition and modelling of gas inertia are given first to demonstrate its ability to mitigate power fluctuations. Since partial utilization of gas inertia can influence overall gas network parameters, the gas network is modelled with an analysis of network dynamic changes. A multi-energy inertia-based power support model and strategy are then proposed for fully using gas-thermal inertia resources in integrated energy systems. The influence of gas network constraints on strategy, economy and power outputs is analyzed. Special circumstances where the gas network can be simplified are introduced. This improves the response speed and application value. The feasibility and effectiveness of the proposed strategy are assessed using a real scenario.

Keywords Gas network, Multi-energy inertia, Power support, Integrated energy system

1 Introduction

With increasing access of renewable energy to the power system, the uncertainty of the output power from renewable energy sources may reduce the reliability of power grid operation [1, 2]. Currently, there is exploration of the potential for ensuring continuous and reliable power supply using energy reserves such as wind power or solar energy [3, 4]. Given the flexibility to realize the conversion of various energy sources [5, 6], an integrated energy system (IES) can also be adopted to provide power support after disturbances [7]. The electricity power can be converted from other energy forms with configurations such as combined heat and power (CHP) units to support power shortages [8, 9], or converted into heat or gas for storage to absorb excess electricity in the power system [10].

*Correspondence:
Qi Wang
wangqi@seu.edu.cn
[1] School of Electrical Engineering, Southeast University, No.2 Sipailou (Southeast University), Xuanwu District, Nanjing, Jiangsu, China

In addition to direct energy conversion, inertial resources contained in slow-dynamic thermal and gas systems in IESs can also resist power fluctuations and support power shortages. For thermal systems, there is a lot of research on the storage potential of district heating networks [9]. As thermal power can be extracted from thermal sources without significantly influencing heat consumers [11], this has led to many studies focusing on the combined use of thermal inertia and demand response [12]. Current modelling methods of thermal inertia are relatively mature, and so will be used directly in our work.

However, for a gas system, the modelling methods of gas inertia still lack sound solutions. Most research focuses on gas storage characteristics, referring to the natural gas remaining in pipelines because of pressure difference between pipe heads and ends [13]. It has been shown that gas storage can be released in a short time for short-term power support [14], or integrated with the electrical power system to deal with uncertain power supply in IESs [15]. Given the similar resistance characteristics of a gas system to power fluctuations as thermal inertia, a similar concept of gas inertia is proposed. As well as gas storage characteristics, reference [16] further enriches the definition of gas inertia by including a gas system's long-time response to the demand changes in the gas inertia characteristics. Nevertheless, despite the expansion of the gas inertia definition, the corresponding mathematical forms have not been given to verify the newly proposed characteristics. Therefore, this paper presents a novel gas inertia model with an intuitive mathematical form to represent both the gas storage's capability to mitigate the power impact, and gas its long-time response capability to delay the impact arrival time.

As for the application scenarios of natural gas system resistance characteristics, gas storage is often used in emergency power support and frequency stability maintenance. Gas storage can support emergent power shortage in seconds along with thermal inertia [17], or maintain frequency stability in minutes, serving as a backup energy for frequency second dip suppression [18]. To simplify the network modelling and improve the computing speed of optimization strategies, gas storage is only considered as an output energy form with the network influence and interactions between pipelines being overlooked [17–19]. To consider the gas network's influence on system operation, the mutual constraint relationship between nodal pressure and gas flow in the gas network is included in [20], and the flow difference between pipe heads and ends brought by consideration of gas storage is included in [21]. Improvements are further made in [22] with concrete analysis of natural gas usage effects on power/gas loads as well as the storage in pipelines.

It can be seen that research on natural gas systems tends to develop towards the refinement of modelling of internal gas networks. Thorough consideration of gas network constraints will inevitably increase the complexity of system operational modelling and reduce computing speed. These are especially influential in emerging power support scenarios. Therefore it is necessary to clarify the influence of partial gas inertia use on overall gas network power support capacity, so as to study gas network simplification conditions. Refinement of modelling of internal gas networks and consideration of scenario applicability of the power support strategies are first examined in this paper. Different from the aforementioned research, the power support strategy proposed in this paper not only considers gas network constraints in detail, but also gives conditions where gas network constraints can be simplified to ensure the practicability of the strategy in real application.

Therefore, based on the intuitive mathematical modelling of gas inertia resistance characteristics, this paper aims at fully using multi-energy inertia resources in power support optimization, and, in particular, refers to thermal energy inertia and natural gas energy inertia in IESs. For thermal inertia, the supply of thermal power at the load side can be reduced to support the electric power shortages. Thus, the influence of power fluctuations on the power balance of electric power system can be reduced by using the resistance ability of the thermal system to power fluctuations. For gas inertia, the pre-reserved gas storage in gas pipelines can be released quickly to support electric power shortages by energy conversion. The influence of power fluctuations on the power balance of electric power system can be reduced by the inertia characteristics of natural gas systems. Then, the strategy of economy and power output are compared in scenarios of considering/not considering gas network constraints. The different power support results confirm the necessity of gas network constraints consideration, while the size of the difference varies with different IES parameters and power shortage conditions. Through the analysis of possible influence factors, conditions whereby gas network constraints can be simplified are given. These involve the power shortage spots in the network and the upper limits of thermal inertia.

The major contributions of this paper are as follows:

1. The capability to accommodate power fluctuations using gas inertia is presented by solving the gas inertia model. To fully use the inertial resources contained in IESs, gas inertia is used along with thermal inertia to support power shortages with improved efficiency.
2. A novel multi-energy inertia-based power support strategy considering gas network constraints is proposed. The strategy of economy and power output are precisely evaluated by analysis of gas network dynamic changes.
3. Since detailed consideration of gas network constraints can increase the computational burden of a power support strategy, certain circumstances where the network can be simplified are introduced. The simplification can reduce modelling complexity and increase computing speed to improve the speed of power support response.

The rest of the paper is organized as follows. Section 2 presents the definition of gas inertia in contrast to thermal inertia, and the modelling of gas inertia to reveal its resistance characteristics. Section 3 establishes the power support model using gas-thermal inertia of IESs with detailed consideration of gas network dynamic changes, and a power support strategy is then proposed with precise measurement of gas storage consumption throughout networks. The feasibility, effectiveness and application value of the proposed strategy are tested in Sect. 4, and Sect. 5 draws the conclusions.

2 Use of gas inertia considering network influence

Given that the two approaches have similar resistance characteristics to power fluctuations, the definition of gas inertia in contrast to thermal inertia is presented in Sect. 2.1. A novel gas inertia model is then established representing both its capability to mitigate the power impact and delay the impact arrival time in an intuitive mathematical form in Sect. 2.2. With further consideration of the internal gas network constraints, a refined modelling of a gas network is presented in Sect. 2.3.

2.1 Definition of gas inertia

For a natural gas system shown in Fig. 1, gas inertia deals with power fluctuations by restoring/releasing gas storage in pipelines depending on the input and output flow difference. With load fluctuations, gas inertia mainly manifests as the response delay of the arrival of the minimum gas pressure and the available gas storage.

The definition of gas inertia is shown in Fig. 1b, while thermal inertia is shown in Fig. 1a. When the input power fluctuates on the thermal sources, thermal inertia mainly manifests as: (1) the response delay of the arrival of the minimum indoor temperature; and (2) the comfort range within which temperature is allowed to change. Therefore, the load fluctuation in a gas system is equivalent to the input power fluctuation in the thermal system, and the slow-speed response of gas pressure at pipe ends in a gas system is equivalent to the slow-speed response of indoor temperature in a thermal system.

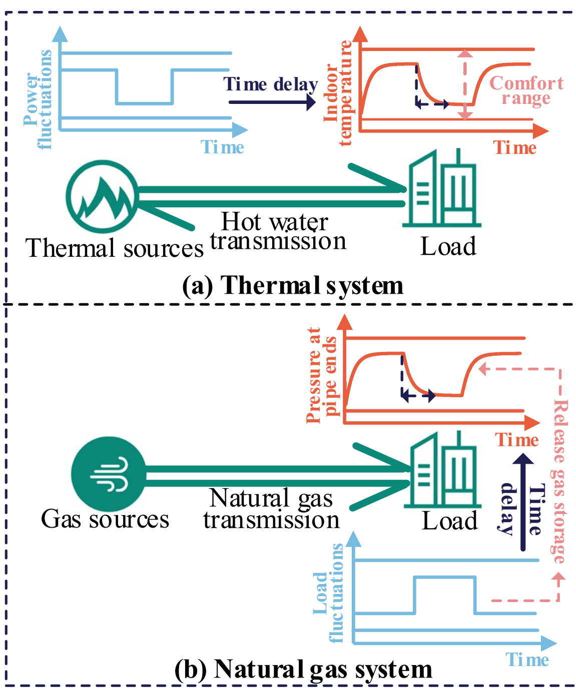

Fig. 1 Definition of gas inertia in contrast to thermal inertia

2.2 Modelling of gas inertia

From the response characteristics providing buffer space for power fluctuations, the power support model of gas inertia based on the dynamic model of a gas system is established.

The relationship between the natural gas pressure, density and pipeline flow can be expressed as [23]:

$$\begin{cases} P^G = R_M T^G \rho \\ q^G = \rho v^G A \end{cases} \tag{1}$$

where $P^G/q^G/T^G$ are the pressure/flow rate/temperature of natural gas. R_M is the quotient of gas constant to molar mass, ρ is the density of natural gas, v^G is the velocity of natural gas, and A is the cross-sectional area of the gas pipe.

The transient transmission process of a gas pipeline can be expressed as [24]:

$$\begin{cases} \frac{\partial \rho}{\partial t} + \frac{\partial \rho \upsilon^G}{\partial x} = 0 \\ \frac{\partial \rho \upsilon^G}{\partial t} + \frac{\partial \rho (\upsilon^G)^2}{\partial x} + \frac{\partial P^G}{\partial x} + \frac{\lambda \rho (\upsilon^G)^2}{2D} + \rho g \sin\theta = 0 \end{cases} \tag{2}$$

where x is the space variable and t is the time variable. θ is the inclination of the pipe to the horizontal plane, D is the inner diameter of pipe, and g is the acceleration due to gravity.

To simplify the dynamic model of a natural gas pipe after the substitution of (1) into (2), the following assumptions are made: a) the differential term v^2 is ignored given its small influence on the gas pressure; and b) θ is considered to be 0.

$$\begin{cases} A \frac{\partial P^G}{\partial t} + R_M T^G \frac{\partial q^G}{\partial x} = 0 \\ \frac{1}{A} \frac{\partial q^G}{\partial t} + \frac{\partial P^G}{\partial x} + \frac{\lambda v^G}{2DA} q^G = 0 \end{cases} \tag{3}$$

The gas pressure response of pipe ends is the direct reflection of gas inertia dealing with load fluctuations. This can be expressed through the simplification of a finite element approximation, as:

$$\frac{AL^G}{R_M T^G} \ddot{P}^G_{out}(t) + \frac{A\lambda v^G L^G}{2DR_M T^G} \dot{P}^G_{out}(t) + \frac{A}{L^G}\left[P^G_{out}(t) - P^G_{in}\right] = -\dot{q}^G_{out}(t) - \frac{\lambda v^G}{2D} q^G_{out}(t) \tag{4}$$

where L^G is the length of the natural gas pipeline, $q^G_{out}(t)/P^G_{out}(t)$ are the flow rate/pressure of pipeline outlet at time t, and P_{in}^{G} is the pressure of pipeline inlet and assumed to be constant.

Assuming the load demand increases instantaneously at t_1 and the gas flow at pipe ends drops from the normal value q_1^G to q_2^G, the process can be expressed as:

$$q_{out}^{G}(t-t_1)=(q_2^G-q_1^G)\varepsilon(t-t_1)+q_1^G \tag{5}$$

where q_1^Gandq_2^G are the initial and dropped values of gas flow rates, and $q_{out}^{G}(t-t_1)$ is the flow rate of the gas pipe outlet at time $t-t_1$.

Substituting (5) into (4) through calculation methods of Laplace/inverse Laplace transforms, the power support model of gas inertia based on the gas pressure response of pipe ends can be obtained as:

1. $a_1=AL^G/(R_M T^G)$;
2. $a_2=A\lambda v^G L^G/(2DR_M T^G)$;
3. $a_3=A/L^G$;
4. $b_1=\lambda v^G/(2D)$;
5. $b_2=AP_{in}^G/L^G$;
6. $P_{out}^G(0^-)=\dot{P}_{out}^G(0^-)=0$;
7. $-x_1$ and $-x_2$ are the two roots of the equation $a_1s^2+a_2s+a_3=0$.

$$P_{out}^G(t)=\left(b_2-b_1q_2^G+b_1q_1^G\right)\Big/(a_1x_1x_2) - \left\{\begin{array}{l}\left[(x_1-b_1)\left(2q_1^G-q_2^G\right)-b_2\right]e^{-x_1t}\Big/x_1\\ -\left[(b_1-x_2)\left(2q_1^G-q_2^G\right)+b_2\right]e^{-x_2t}\Big/x_2\end{array}\right\}\Big/\left[a_1(x_2-x_1)\right] \tag{6}$$

where $x_1\geq 0$ and $x_2\geq 0$, and are given by:

$$\begin{aligned}x_1&=\left(a_2/a_1-\sqrt{(a_2/a_1)^2-4a_3/a_1}\right)\Big/2\geq 0\\ x_2&=\left(a_2/a_1+\sqrt{(a_2/a_1)^2-4a_3/a_1}\right)\Big/2\geq 0\end{aligned} \tag{7}$$

The above gas inertia model reveals its support capability in response to abrupt power shortages. The negative exponential function form of gas inertia response mitigates the step function form of power fluctuations and delays the arrival of a power fluctuation shock to the system. Enough buffer space is provided to deal with power shortages. This establishes the foundation for gas inertia utilization in the power support strategy.

2.3 Modelling of natural gas network

The utilization of gas inertia mainly manifests as the use of gas storage, which involves the change of pressure, flow rate and gas storage of multiple gas pipelines in the network. Therefore, gas inertia providing support to power shortages at one load might influence the use of gas inertia at other loads, leading to their consequent decrease in power support capability.

This paper adopts a typical 8-node gas network structure shown in Fig. 2 to analyze the network influence on gas inertia utilization. The gas network is supplied by two gas sources GS_1 and GS_2. Three load groups Load 1 L_1, Load 2 L_2 and Load 3 L_3 are connected respectively at the end of the gas pipes 12, 34, and 67. The corresponding gas flows at the load groups are q_{L1}^G, q_{L2}^G and q_{L3}^G, respectively. The gas flows at the head/end of the gas pipe mn are $q_{mn,in}^G/q_{mn,out}^G$, the pressures of natural gas at nodes m/n are P_m^G/P_n^G, and the gas storage in the gas pipe mn at time t is $V_{mn}^G(t)$.

The gas storage is defined as a certain amount of gas stored in the pipeline because the quantities of incoming and outgoing flows may differ [22]. The gas storage within a gas pipe from node m and node n at time t can be expressed as:

$$V_{mn}^G(\mathrm{t})=\frac{\pi}{4}\frac{L_{mn}^G d_{mn}^G}{R_M T^G Z\rho_0}\overline{P}_{mn}^G(\mathrm{t}) \tag{8}$$

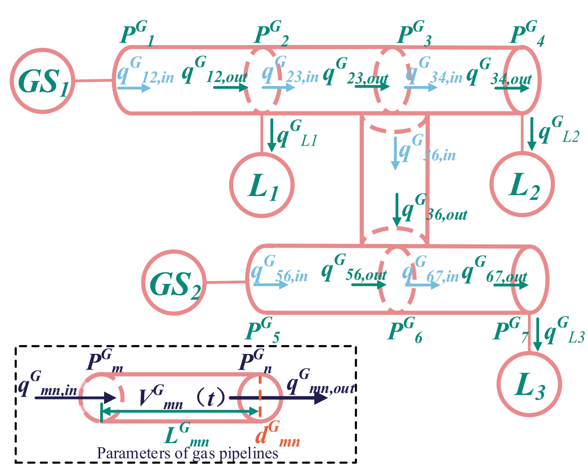

Fig. 2 The 8-node gas network structure diagram and relevant parameters of gas pipelines

where ρ_0 is the density of natural gas under standard conditions (0.7174 (kg/m^3)). L_{mn}^G/d_{mn}^G are the length/diameter of the gas pipe mn, and $\overline{P}_{mn}^G(t) = (P_m^G + P_n^G)/2$ represents the average gas pressure in the pipeline.

The change of the gas storage amount from time $t-1$ to time t can be expressed as:

$$V_{mn}^G(\mathrm{t}) - V_{mn}^G(\mathrm{t}-1) = q_{mn,in}^G(\mathrm{t}) - q_{mn,out}^G(\mathrm{t}) \tag{9}$$

where $V_{mn}^G(t-1)$ is the gas storage in the gas pipe mn at time $t-1$, and $q_{mn,in}^G(t)/q_{mn,out}^G(t)$ are the gas flows at the head/end of the gas pipe mn at time t.

Usually, the relationship between the gas pressure and flow in the static natural gas system between node m and node n without compressors is given as (10):

$$\left(P_m^G\right)^2 - \left(P_n^G\right)^2 = 1.62\lambda\rho_0 P_0^G \frac{T^G}{T_0^G}\frac{Z}{Z_0^G}\frac{L_{mn}^G}{\left(d_{mn}^G\right)^5}\left(q_{mn}^G\right)^2 \tag{10}$$

where P_0^G and T_0^G are the pressure (101.325 kPa) and temperature (278 K) of natural gas under standard conditions, respectively. Z_0^G is the compression factor of natural gas under standard conditions, and Z is the compression factor of natural gas. q_{mn}^G is the flow rate of natural gas in pipe *mn*.

When considering gas storage and accompanying gas flow difference between pipe heads and pipe ends, Eq. (10) should be replaced by:

$$\left(P_m^G\right)^2 - \left(P_n^G\right)^2 = 1.62\lambda\rho_0 P_0^G \frac{T^G}{T_0^G}\frac{Z}{Z_0^G}\frac{L_{mn}^G}{\left(d_{mn}^G\right)^5}\left(\overline{q}_{mn}^G\right)^2 \tag{11}$$

where $\overline{q}_{mn}^G = (q_{mn,in}^G + q_{mn,out}^G)/2$ represents the average gas flow in the pipeline.

Based on the above gas network modelling, the condition of gas storage consumption is presented in detail through the flow rate changes of pipelines in Fig. 3. The power shortages occur at L_1, L_2 and L_3. Gas storage is increased when the flow rate at pipe heads is greater than the flow rate at pipe ends and is consumed when the flow rate at pipe heads is less than that at pipe ends. The flow rate of natural gas at the loads usually remains consistent with the change in load, and only changes when the load demand changes.

Since the three fault cases in Fig. 3 follow the same natural gas dynamic change mechanism, the case of power shortages at L_1 shown in Fig. 3a is chosen as an example to be explained in detail. To support power shortages at L_1, the electricity demand will increase suddenly, resulting in a sudden increase in the flow rate at L_1 and Node 2. During this process, the flow rate at Node 1 is less than that of Node 2, suggesting that the gas storage in pipe12 is consumed. Following this principle, the gas storage is also consumed in pipe23, pipe34, pipe36 and pipe67 during power shortages at L_1. When the power shortages disappear, the flow rate at L_1 returns to normal and the flow rate at Node 1 is greater than that of Node 2, suggesting that the gas storage in pipe12 is increased. Following this principle, the gas storage in pipe23, pipe34, pipe36 and pipe67 is also increased after the recovery of power shortages. In summary, the following three phenomena are illustrated by Fig. 3:

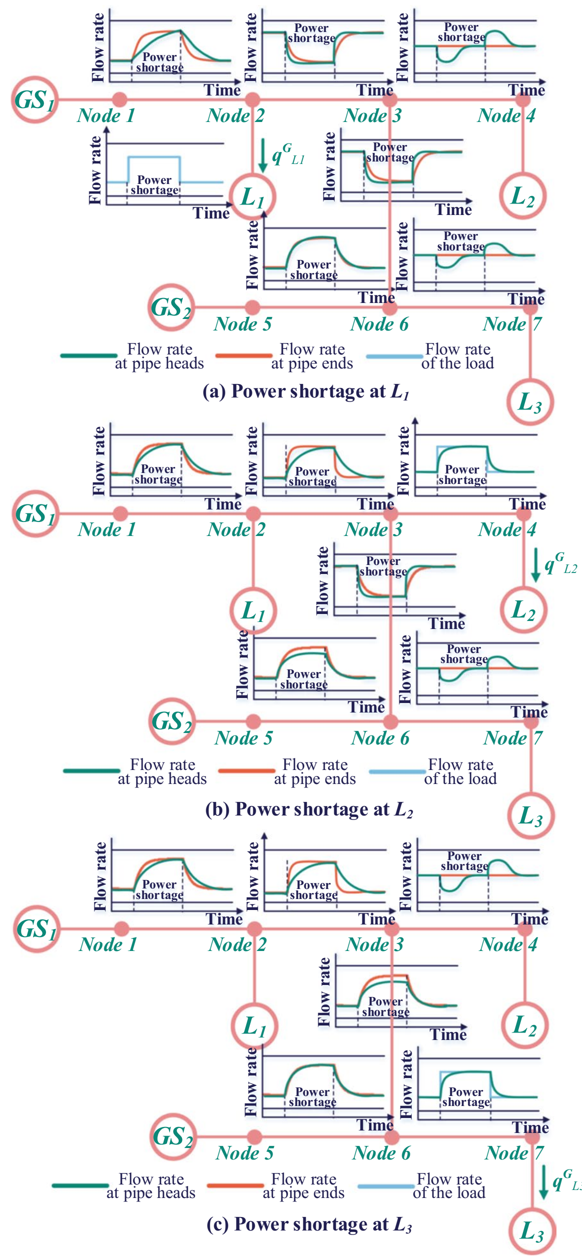

Fig. 3 Flow rate variations in gas network pipelines with power shortages at L_1, L_2 and L_3

1. Most pipelines will contribute a portion of gas storage at the beginning of power shortages and then slowly store the natural gas at the end of power shortages.
2. Power shortages at one load not only consume the gas storage in the nearby pipelines, but also influence the amount of gas storage in the whole gas network. This can further affect the usage of natural gas by other loads as well as reduce their power support potential if not regulated.
3. Power shortages at different load spots have different gas storage consumption results. This suggests the need to study different power shortage spots in the network.

Therefore, it is important to consider the network influence of a natural gas system in the use of gas inertia.

3 Power support model of multi-energy inertia considering gas network constraints

During power grid operation, power fluctuations often occur because of the imbalance between power supply and demand. Current methods of supporting power shortages usually focus on the exclusive use of inertial resources in IESs, whereas the similar characteristics to resist power fluctuations between different inertial resources can be further explored and applied in multi-energy inertia-based power support to improve the efficiency of IES operation. Despite the joint use of gas inertia with other energy forms in some research, the gas network is often considered as an entirety with the internal dynamic changes and consequent influences being overlooked. Therefore, this section introduces a new power support strategy considering multi-energy inertial resources in gas and thermal systems. The gas network is modelled in detail with load groups connected to different locations. Use of gas inertia is likely to affect the normal operation of load groups without power shortages. Therefore, the output of different energy forms and power support strategy economy will be different from when the gas network is considered as an entirety.

As for the network influence of a thermal system, since the support time scale of thermal inertia is up to hours compared with the minute-level of gas inertia, the dynamic changes of a natural gas network is much larger than that of thermal network over the same power support time. Therefore, the network influence of thermal system will not be considered in detail in this paper.

3.1 Internal structure of the integrated energy system

The internal structure of IESs studied in the paper is shown in Fig. 4, where two gas sources and N groups of

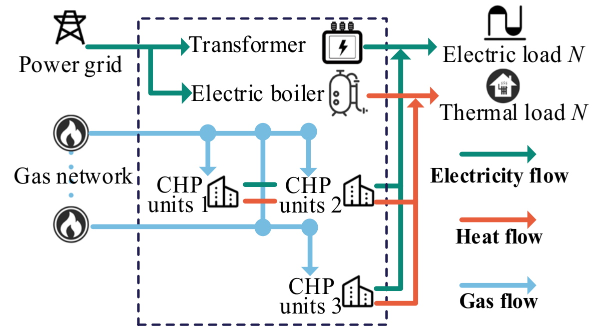

Fig. 4 Internal structure of the IES

loads ($N = 1, 2, 3$) are presented with the 8-node gas network structure of Fig. 2. Three types of energy are involved in this multi-energy system, i.e., thermal, natural gas and electric. The electric load is supplied by the external power grid and CHP units of the respective load groups, while the thermal load is supplied by the electric boiler and CHP units of the respective load groups. The input and output model of the energy hub is given as:

$$\begin{bmatrix} L_n^E \\ L_n^H \end{bmatrix} = \begin{bmatrix} \lambda_{dis}^E \eta_T & \eta_{L_n}^{CHPE} \\ (1-\lambda_{dis}^E)\eta_{EB} & \eta_{L_n}^{CHPH} \end{bmatrix} \cdot \begin{bmatrix} P^{ES} \\ P_1^{GS} + P_2^{GS} \end{bmatrix} \tag{12}$$

where L_n^E/L_n^H is the electric load/thermal load of L_n (n = 1, 2, 3). λ_{dis}^E is the electric energy distribution coefficient. η_T/η_{EB} is the transformer/electric boiler conversion efficiency, and $\eta_{L_n}^{CHPE}/\eta_{L_n}^{CHPH}$ is the gas-electricity/gas-heat conversion efficiency of the CHP units of L_n (n = 1, 2, 3). P_1^{GS}/P_2^{GS} are the external gas sources 1 and 2, while P^{ES} is the external power supply.

3.2 Gas-thermal inertia-based power support strategies considering gas network constraints

Supposing the power shortages occur at one load group in the IES, gas and thermal inertia mainly respond in two ways involving the transmission or conversion of the three energy forms of electric, thermal and gas, as:

1. To make up for the power shortages at one load, electricity from the power grid can be directly rearranged to supply the electric load from the original route of the electric boiler. This method requires no conversion of any energy but only the control centre to rearrange the power transfer route. This method will lead to the decrease of thermal power on the load side, but is still feasible because of the existence of thermal inertia. Therefore, although this method is essentially the transmission of electrical energy, it is called thermal inertial output.

2. To obtain more electricity within a short time, natural gas stored in gas pipelines can be converted to electricity through CHP units. This method takes advantage of the fast response speed of CHP units and pre-stored gas storage at the expense of increased thermal power from the output of CHP units.

During the power support process, thermal power on the load side may decrease because of the first method but increase because of the second method. The total thermal deviation caused by the two methods can affect the user comfort on the load side, but with a time delay, while it mitigates power fluctuations and temperature-tolerance from the users given the existence of thermal inertia. Gas inertia mainly contributes to the pre-stored gas storage and the delayed-response of gas pressure, which delays the time of the pipe pressure reaching the lower limit and allows more time for the power support provided from gas inertia.

The influence of the gas network is studied based on the 8-node gas network structure shown in Fig. 2 with three load groups connected to different spots. Assuming that the power shortages occur at L_1, three output forms are considered in the whole power support process as shown in Fig. 5:

1. Gas inertia output uses gas storage from different pipelines in the gas network to support the electricity shortages at L_1 through the single CHP unit at L_1.
2. The electricity transferred from the electric boiler to the transformer may come from three different load groups, called the thermal inertia output given that the feasibility of this method is to make use of: (a) the tolerance of load side to temperature change; (b) the time delay; and (c) the reduced fluctuation influence of the thermal source on the load side.
3. Given thermal fluctuations resulting from gas-thermal inertia output on the load side, the demand side output is also considered based on users' willingness to tolerate total thermal deviation on the load side brought by various power support methods.

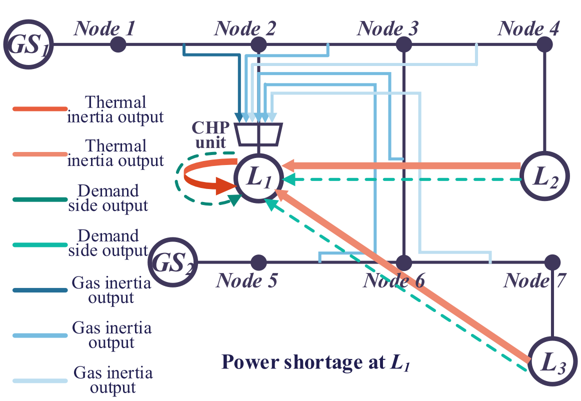

Fig. 5 Working mechanism of three output forms in the power support process

The above three output forms act simultaneously in no particular order while there are differences in the unit output costs between the same output form. These are marked with different colours in Fig. 5. The main response force among the three load groups should be L_1 and the pipelines nearby when the power shortages are at L_1. Therefore, when the outputs of other load groups are mobilized because of the failure of L_1, it may affect their normal operation and even the ability to deal with possible power failure in the future, so the unit cost of output would increase.

3.3 The objective function

This paper deals with power shortages using power support from gas-thermal inertia. To ensure the system reliability level, the objective function is to minimize the total cost of the power support during the power failure period, given as:

$$\min Cost = C_{RG} + C_{RH} + C_{COM} + C_{CHP} \tag{13}$$

where $Cost, C_{RG}, \text{and} C_{CHP}$ are the total cost, and costs of gas inertia output, thermal inertia output, demand side output, and heat-electricity ratio adjustment, respectively.

The calculation methods for the different costs are shown as:

$$\begin{aligned} C_{RG} = {} & c^1_{RG,L_n}\left[\begin{array}{l}\left|V^G_{12}(t_0) - V^G_{12}(t_0+T)\right| \\ +T\left|q^G_{12}(t_0+T) - q^G_{12}(t_0)\right|\end{array}\right] \\ & + c^2_{RG,L_n}\left|V^G_{23}(t_0) - V^G_{23}(t_0+T)\right| \\ & + c^3_{RG,L_n}\left|V^G_{34}(t_0) - V^G_{34}(t_0+T)\right| \\ & + c^4_{RG,L_n}\left[\begin{array}{l}\left|V^G_{56}(t_0) - V^G_{56}(t_0+T)\right| \\ +T\left|q^G_{56}(t_0+T) - q^G_{56}(t_0)\right|\end{array}\right] \\ & + c^5_{RG,L_n}\left|V^G_{67}(t_0) - V^G_{67}(t_0+T)\right| \\ & + c^6_{RG,L_n}\left|V^G_{36}(t_0) - V^G_{36}(t_0+T)\right| \end{aligned} \tag{14}$$

$$C_{RH} = \sum_{t=t_0}^{T}\left[c^1_{RH,L_n}P^1_{RH}(t) + c^2_{RH,L_n}P^2_{RH}(t) + c^3_{RH,L_n}P^3_{RH}(t)\right] \tag{15}$$

$$C_{COM}=\sum_{t=t_0}^{T}\left[\sum_{c=1}^{C}\sum_{m=1}^{M}\mathrm{c}_{COM,L_n}^{c,m}\left|e_{heat}^{c,m}(t)\right|\right] \tag{16}$$

$$C_{CHP}=\sum_{t=t_0}^{T}\sum_{\mathrm{w}=1}^{W}c_{CHP}^{w}P_{RG}^{\mathrm{n}w}(t)\; n=1,2,3 \tag{17}$$

where T is the duration of the power shortage, and t_0 is the initial time of the power shortage occurrence. $c_{RG,L_n}^{a}c_{RG,L_n}^{b}$ are the respective unit costs of gas storage in pipe $a(a+1)$ and pipe $(b+1)(b+2)$ with power shortages at L_n (a=1, 2, 3; b=4, 5). c_{RG,L_n}^{6} is the unit cost of gas storage in pipe 36 with power shortages at L_n (n = 1, 2, 3), and c_{RH,L_n}^{c} is the unit cost of thermal inertia at L_c with power shortages at L_n (c, n = 1, 2, 3). $c_{COM,L_n}^{c,m}$ is the unit cost of demand side output of L_c in level m with power shortages at L_n (c, n = 1, 2, 3), while c_{CHP}^{w} is the unit cost of heat-electricity ratio adjustment in level w. $P_{RH}^{c}(t)$ is the power output of thermal inertia of L_c at time t (c = 1, 2, 3), $P_{RG}^{n,w}(t)$ is the power output of gas inertia in level w at time t, and $L_n e_{heat}^{c,m}(t)$ is the thermal deviation of L_c in level m at time t (c = 1, 2, 3)., M is the total level of demand side step price, W is the total level of heat-electricity ratio adjustment step price, and C is the total load group (C = 3).

Among these costs, the unit costs of gas and thermal inertia are fixed prices, which are set according to the spot of power shortages and load groups. The unit cost of thermal inertia output from other load groups will be higher than that of the power shortage location. The unit cost of gas inertia output from the pipelines far from the power shortage spot will be higher than that in the nearby pipelines of the power shortage spot, and will be even higher if the end of the pipeline is directly connected to other load groups given that the possibility of affecting the normal gas supply of other loads will increase.

The demand side output adopts the step price and is divided into M response levels, where M is the total step number of demand side step price. When one load group is operating normally and needs to provide demand side output for other loads with power shortages, the demand side step price is higher than that in the power shortage spot.

CHP units usually have an optimal heat-electricity ratio, under which the energy utilization rate is the highest, and the generated thermal power and increased fuel consumption are optimally balanced. The optimal heat-electricity ratio is 1.0 in this paper, and the corresponding heat-electricity ratio adjustment cost is the lowest given its highest energy utilization rate. When the heat-electricity ratio is increased for more thermal power, the heat-electricity ratio adjustment cost at the same gas consumption will also increase. Therefore, consumption of gas under different heat-electricity ratios corresponds to different prices. The heat-electricity ratio adjustment cost adopts the step price and is divided into W response levels, where W is the total step number of heat-electricity ratio adjustment cost.

3.4 The constraint conditions

1. Electrical power balance constraint

$$P_{RG}^{n}(t)\eta_{L_n}^{CHPE}+\left[P_{RH}^{1}(t)+P_{RH}^{2}(t)+P_{RH}^{3}(t)\right]\eta_T=e_{ele}(t) \tag{18}$$

where $P_{RG}^{n}(t)$ is the power output of gas inertia at L_n at time t, and $e_{ele}(t)$ is the electric power shortage at time t, where t is between t_0 and T. The electric power shortages are supported by the electricity output of CHP units and the transfer of electricity from the three load groups.

2. Thermal power balance constraints

Based on the principle of minimizing the influence of power support on the normal operation of other load groups, only the CHP unit in the power shortage spot consumes the gas storage in response to the power shortages. Therefore, different power shortage spots correspond to different responding CHP units. Supposing the power shortages are at L_G:

$$\begin{cases}\left|P_{RG}^{G}(t)\eta_{L_G}^{CHPH}-P_{RH}^{G}(t)\eta_{EB}\right|=e_{heat}^{G}(t) & (1\le G\le 3)\\ \left|P_{RH}^{K}(t)\eta_{EB}\right|=e_{heat}^{K}(t) & (1\le K\le 3, K\ne G)\end{cases} \tag{19}$$

Thermal deviation at L_G is caused by the increased heat output of CHP units at L_G and the reduced electricity of electric boilers at L_G, whereas thermal deviations at L_K are caused by the reduced electricity of electric boilers at L_K.

3. Total gas inertia output constraint

$$\mathrm{q}_{L_\mathrm{n}}^{G,m}(\mathrm{t})-\mathrm{q}_{L_\mathrm{n}}^{G,m}(\mathrm{t_0})=\frac{\sigma_{\mathrm{conv}}P_{RG}^{n}(t)}{1000H_{\mathrm{gas}}}\quad n=1,2,3 \tag{20}$$

where $q_{L_n}^{G,m}(t)$ and $q_{L_n}^{G,m}(t_0)$ are the gas flow of L_m at time $t$andt_0 with power shortages at L_n (m, n = 1, 2, 3), respectively. σ_{conv} is the conversion coefficient from 'kWh' to 'J', and H_{gas} is the calorific value of gas. Different measuring units of $P_{RG}^{n}(t)$ and $q_{L_n}^{G,m}(t)$ are unified using (22) shown below.

4. Gas flow, pressure and storage related constraints
   The gas flow, pressure and storage related constraints are the extensions of the abovementioned (8), (9), and (11), given as:

$$\begin{cases} V_{mn}^G(\mathrm{t}) = \frac{\pi}{4}\frac{L_{mn}^G d_{mn}^G}{R_M T^G Z\rho_0}\frac{P_{\mathrm{m}}^G(\mathrm{t})+P_n^G(\mathrm{t})}{2} \\ \left[P_m^G(t)\right]^2 - \left[P_n^G(t)\right]^2 \\ \quad = 1.62\lambda\rho_0 P_0^G \frac{T^G}{T_0^G}\frac{Z}{Z_0^G}\frac{L_{mn}^G}{(d_{mn}^G)^5}\left[\frac{q_{mn,in}^G(t)+q_{mn,out}^G(t)}{2}\right]^2 \\ V_{mn}^G(t_0) = V_{mn}^G(t_0 - T) + T\left[q_{mn,in}^G(t_0) - q_{mn,out}^G(t_0)\right] \end{cases} \tag{21}$$

5. Nodal flow of natural gas constraints

The nodal flow of natural gas is similar to the nodal flow of electricity and follows the principle that the total incoming flow at the node equals the total outcoming flow. The flow rate of natural gas at the loads remains consistent with the change in load, and changes only when the load demand changes.

When the power shortages are at L_1, $q_{L_1}^{G,2}(t)$ and $q_{L_1}^{G,3}(t)$ remain the same:

$$\begin{cases} q_{12,out}^G(t) = \mathrm{q}_{L_2}^{G,1}(\mathrm{t}_0) + q_{23,in}^G(t) \\ q_{23,out}^G(t) = q_{36,in}^G(t) + q_{34,in}^G(t) \\ q_{56,out}^G(t) + q_{36,out}^G(t) = q_{67,in}^G(t) \\ q_{34,out}^G(t) = \mathrm{q}_{L_2}^{G2}(\mathrm{t}) \\ q_{67,out}^G(t) = \mathrm{q}_{L_2}^{G3}(\mathrm{t}_0) \end{cases} \tag{22}$$

When the power shortages are at L_2, $q_{34,out}^G(t)$ changes with $q_{L_2}^{G,2}(t)$ while $q_{L_2}^{G,1}(t)$ and $q_{L_2}^{G,3}(t)$ remain the same:

$$\begin{cases} q_{12,out}^G(t) = \mathrm{q}_{L_2}^{G,1}(\mathrm{t}_0) + q_{23,in}^G(t) \\ q_{23,out}^G(t) = q_{36,in}^G(t) + q_{34,in}^G(t) \\ q_{56,out}^G(t) + q_{36,out}^G(t) = q_{67,in}^G(t) \\ q_{34,out}^G(t) = \mathrm{q}_{L_2}^{G2}(\mathrm{t}) \\ q_{67,out}^G(t) = \mathrm{q}_{L_2}^{G3}(\mathrm{t}_0) \end{cases} \tag{23}$$

For power shortages at L_3, $q_{67,out}^G(t)$ changes with $q_{L_3}^{G,3}(t)$ while $q_{L_3}^{G,1}(t)$ and $q_{L_3}^{G,2}(t)$ remain the same, as:

$$\begin{cases} q_{12,out}^G(t) = \mathrm{q}_{L_3}^{G,1}(\mathrm{t}_0) + q_{23,in}^G(t) \\ q_{23,out}^G(t) = q_{36,in}^G(t) + q_{34,in}^G(t) \\ q_{56,out}^G(t) + q_{36,out}^G(t) = q_{67,in}^G(t) \\ q_{34,out}^G(t) = \mathrm{q}_{L_3}^{G2}(\mathrm{t}_0) \\ q_{67,out}^G(t) = \mathrm{q}_{L_3}^{G3}(\mathrm{t}) \end{cases} \tag{24}$$

6. Power output related upper and lower limits constraints

$$\begin{cases} 0 \le P_{RH}^n(t) \le P_{RH,\max}^n \\ 0 \le P_{RG}^n(t) \le P_{RG,\max}^n \end{cases} \tag{25}$$

   where $P_{RH,max}^n$, and $P_{RG,max}^n$ are the upper limits of thermal and gas inertia outputs at L_n ($n=1, 2, 3$), respectively. Both outputs of thermal and gas inertia have upper limits to ensure the safe operation of IESs.
7. Gas related upper and lower limits constraints

$$\begin{cases} V_{mn,\min}^G \le V_{mn}^G(\mathrm{t}) \le V_{mn}^G(\mathrm{t}_0) \\ P_{a,\min}^G \le P_a^G(t) \le P_{a,\max}^G \quad 1 \le a \le 7 \\ P_{c+1}^G(t) \le P_c^G(t) \quad 1 \le c \le 6, c \ne 4 \end{cases} \tag{26}$$

$V_{mn,min}^G$ is the lower limit of gas storage in pipe mn, while $P_{a,min}^G$ and $P_{a,max}^G$ are the lower and upper limits of gas pressure at node a ($1 \le a \le 7$), respectively. Excessive consumption of gas storage will lead to abnormal low nodal pressure, thus affecting the downstream load gas supply.

8. Heat-electricity ratio constraint

$$\eta_{L_n}^{CHPE} \le \eta_{L_n}^{CHPH} \le 0.95 \tag{27}$$

The adjustment range set in this paper is 1.0–1.9 so that the power support model can adjust the heat-electricity ratio of CHP units by itself according to the requirements of the objective function.

4 Case study

This case is simplified from a northern electricity, gas, and heat coupling IES. The typical summer day of the electric power load and thermal load data is shown in Fig. 6, which illustrates the background load condition of the studied IES. Based on this background load condition, the topology structure of the gas network in this

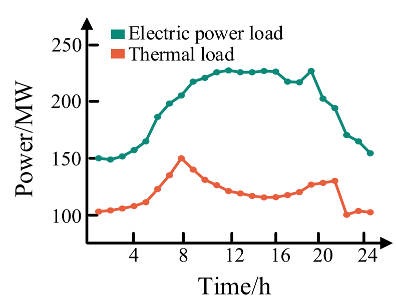

Fig. 6 Background load condition of the studied IES

Table 1 Constant parameters

Symbol	Value
λ	0.0112
T	3600.0000 (s)
T^G	293.1500 (K)
Z_0^G	1.0000
Z	0.9900
R_M	0.5196
η_T	0.9800
η_{EB}	0.9000
$\eta_{L_n}^{CHPE}$	0.5000

Table 2 Parameters of the natural gas network

Symbol	Value
$L_{12}^G/L_{23}^G/L_{34}^G/L_{56}^G/L_{67}^G/L_{36}^G$	6.1000×10^4 (m)
$d_{12}^G/d_{23}^G/d_{34}^G/d_{56}^G/d_{67}^G/d_{36}^G$	0.6000 (m)
P_1^G	6.0000×10^6 (MPa)
P_5^G	5.0000×10^6 (MPa)
$q_{L_1}^G$	27.7778 (N m^3/s)
$q_{L_2}^G$	55.5556 (N m^3/s)
$q_{L_3}^G$	83.3333 (N m^3/s)

Table 3 Unit cost of gas storage c_{RG,L_N}^n (¥/N m^3)

n	$N=1$	$N=2$	$N=3$
1	2.5065	2.9140	2.9140
2	2.7102	2.7102	2.7102
3	2.9140	2.5065	3.0567
4	2.7102	2.7102	2.7102
5	3.0567	3.0567	2.5065
6	2.7102	2.7102	2.7102

Table 4 Unit cost of thermal inertia c_{RH,L_N}^n (¥/N m^3)

n	$N=1$	$N=2$	$N=3$
1	0.2000	0.3500	0.3500
2	0.3500	0.2000	0.3500
3	0.3500	0.3500	0.2000

case adopts the 8-node gas network structure diagram shown in Fig. 2, and is commonly used in related natural gas network research. The internal structure containing the gas network topology of the studied IES is shown in Fig. 4.

Table 5 Step price of demand side output at L_N

Thermal deviation (kWh)	Unit cost with power shortage (¥/kWh)	Unit cost without power shortage (¥/kWh)
0–100	0.1200	0.1320
100–200	0.1500	0.1650
200–300	0.1800	0.1980
> 300	0.2300	0.2530

Table 6 Step price of heat-electricity ratio adjustment

Heat-electricity ratio	Unit cost (¥/kWh)
1.0–1.3	0.0500
1.3–1.5	0.0800
1.5–1.7	0.1100
1.7–1.9	0.1400

All relevant constant parameters are shown in Table 1, and parameters of the gas network are shown in Table 2. The unit costs of gas storage c_{RG,L_N}^n and thermal inertia c_{RH,L_N}^n are shown in Tables 3 and 4, respectively. The demand side output and the heat-electricity ratio adjustment adopt step prices shown in Tables 5 and 6, respectively. The power support optimization is carried out in MATLAB 2019 with the toolbox of YALMIP. The concepts of setting up the next three case studies are as follows:

1. Section 4.1 provides an analysis of the gas network conditions including the changes of gas pressure, gas flow and gas storage under different power shortage spots. Various changes in the gas network verify the value of considering gas network constraints in the power support model, and establish the foundation for the following study.
2. To further prove the significance of considering gas network constraints, the proposed strategy in this paper is compared with similar power support strategies considering the gas network as an entirety [17] in Sect. 4.2.
3. Based on the comparisons in Sect. 4.2, it is found that power shortage spots in the gas network may affect power support results, which are analysed in Sect. 4.3.
4. To improve the application value of the proposed strategy, circumstances are given in Sect. 4.4 where the gas network can be simplified to reduce modelling complexity and increase computing speed.

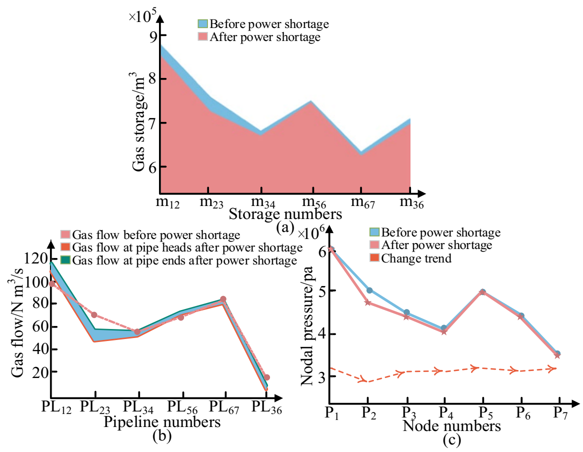

Fig. 7 The network conditions with the power shortages at L_1

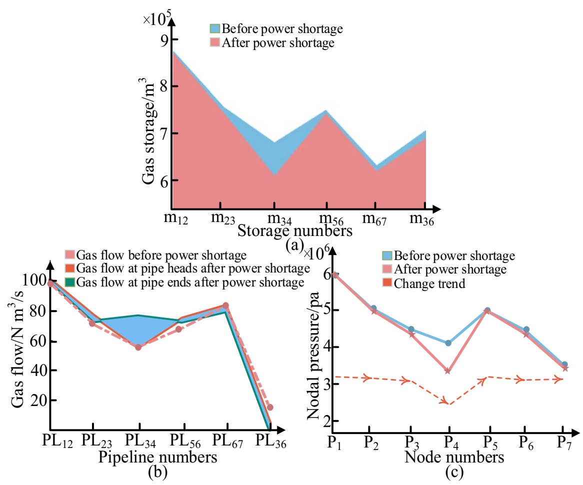

Fig. 8 The network conditions with the power shortages at L_2

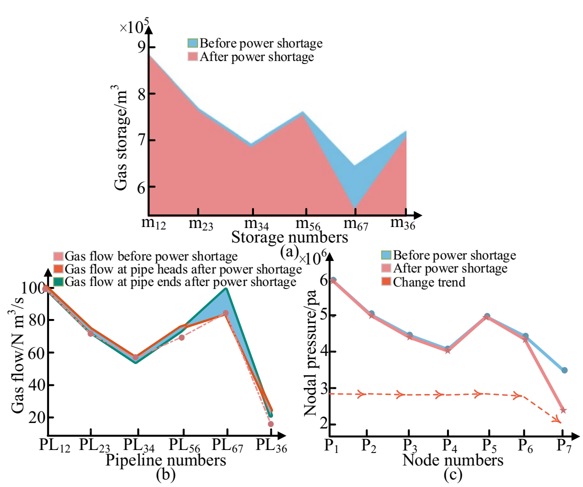

Fig. 9 The network conditions with the power shortages at L_3

4.1 Analysis of the network condition with different power shortage spots

Based on the 8-node gas network structure shown in Fig. 2, the changes of gas pressure, gas flow rate and gas storage in the pipelines of the whole gas network are studied assuming power shortages of 500 kWh/s occurring respectively at L_{1-3} for 3600 s. The network conditions with the power shortages at L_{1-3} are shown in Figs. 7, 8 and 9, respectively. Figures 7a and 8a demonstrate the consumptions of gas storage in each pipe, while Figs. 7b and 8b demonstrate the gas flows in the steady state before power shortages and at pipe heads and ends after power shortages. Figures 7c and 8c demonstrate the changes of gas pressure at different nodes and the corresponding change trends of pressure before and after power shortages. The results of power support regarding costs and outputs of power forms are listed in Table 7a–c.

Instead of considering the gas network as an entirety and focusing only on input and output flows, the parameters of each pipeline can vary in a more complex way when taking into account the gas network. Therefore, the power support model considering unified gas-thermal inertia can be established more comprehensively when the variations are considered in detail in the optimization model.

From Figs. 7a, 8a and 9a, the increase of load demand at one load group will consume gas storage in almost all the pipelines in the network, especially in the pipelines closest to the power shortage spot.

In Figs. 7b, 8b and 9b, the gas flows at pipe heads and ends remain the same in the steady state but deviate after power shortages. Gas inertia output is increased to support power shortages at one load, and this leads to the sudden rise in the gas flow, especially at the end of the pipe where the load group is connected. Therefore, the respective gas flows at the end of the pipes PL_{12}, PL_{34}, and PL_{67} increase more significantly than other flow variations in pipelines when power shortages are at L_1, L_2, and L_3, respectively. The change of flow rate can also reflect the consumption of gas storage by the area between the head and end flows. Gas storage is consumed/stored when the flow rate at pipe heads is smaller/larger than the flow rate at pipe ends. Therefore, the variation trends of the area between the head and end flows in Figs. 7b, 8b and 9b are consistent with the variation trends of the gas storage in Figs. 7a, 8a and 9a.

In Figs. 7c, 8c and 9c, the change of pressure is caused by the variation of gas flow. Since the natural gas flowing out of the pipeline is too fast to be replenished in a short time, the rise in the gas flow will lead to a delayed fall in pressure. The pressure drop at the power shortage spot is particularly large given the largest gas storage supply,

Table 7 Costs and outputs of power forms with power shortages of 500 kWh/s at L_{1-3}

	Cost (¥)	Output
(a) L_1		
Thermal inertia	323,990	100.0000/99.9917/100.0000 (kWh/s)
Gas inertia	387,260	412.0163 (kWh/s)
Demand side	137,380	116.0082/89.9925/90.0000 (kWh/s)
Heat-electricity ratio adjustment	74,163	1.0000
Total	922,780	/
(b) L_2		
Thermal inertia	324,000	100.0000/100.0000/100.0000 (kWh/s)
Gas inertia	386,400	412.0000 (kWh/s)
Demand side	137,380	90.0000/116.0000/90.0000 (kWh/s)
Heat-electricity ratio adjustment	74,160	1.0000
Total	921,940	/
(c) L_3		
Thermal inertia	324,000	100.0000/100.0000/100.0000 (kWh/s)
Gas inertia	379,130	412.0163 (kWh/s)
Demand side	137,380	90.0000/116.0000/90.0000 (kWh/s)
Heat-electricity ratio adjustment	74,160	1.0000
Total	914,670	/

so the lowest point of the pressure change trend before and after power shortages is always at the power shortage spot.

In Table 7a–c, both power forms of thermal inertia and demand side have three outputs representing the outputs from the three load groups. Table 7 shows that power shortages at different spots can result in different total costs and power outputs. Although the difference is not so large with the same failure size and duration, the results still prove the value of considering gas network constraints in the power support model. Next, the proposed strategy is compared with existing power support strategies without full consideration of the gas network constraints [17]. The comparison will further prove the significance of considering gas network constraints.

4.2 Analysis of the strategy comparisons between considering and not considering gas network constraints

Without considering the network influence, the gas network is considered in its entirety and the power support model no longer distinguishes from which pipeline the gas inertia output comes. The unit cost of gas inertia is uniformly set as 2.5065 ¥/(N m^3) while other forms of power support remain the same. The results of the power support strategies considering and not considering gas network constraints are compared in Figs. 10, 11 and 12 with the power shortage occurring at L_{1-3}. The comparison of the total costs between considering and not considering gas network constraints is specifically shown in Table 8.

Table 8 demonstrates the differences of total costs between considering and not considering the gas network constraints. The total costs considering gas network constraints under different sizes of power shortages are all higher than those not considering gas network constraints. The reason is that the unit cost of gas inertia is uniformly set as 2.5065 ¥/(N m^3) in the case of not considering the gas network. This is the lowest in the case of considering gas network. Considering the impact of power shortages at one location on the whole gas network, the unit cost of gas inertia will be increased. Therefore, the total cost considering gas network constraints is bound to rise. However, the changing trend of the total cost difference between considering and not considering gas network constraints *Cost-CostN* in Table 8 shows that *Cost-CostN* is generally lower when the power shortages are small, and begins to increase when the power shortage size reaches a certain degree. This trend implies that under certain circumstances, the size of the total cost can be estimated considering the simplification of gas network constraints. Specific simplified scenarios will be described in the following paragraphs.

Figures 10a and 11a evaluate the power support strategy economy by presenting the total costs of the strategy, with and without considering gas network constraints, under different power shortages. The difference of total costs between considering and not considering the network is also plotted for clearer observation. In general, the total costs considering the network under different power shortages are higher than those without considering the network. The main reason is that the gas inertia unit cost without considering networks is the lowest among all gas inertia unit costs considering networks, while unit costs of the other outputs are the same. However, there is a turning point on the cost difference curve. The cost difference remains unchanged regardless of how much the power shortages are before the turning point, but increases with the increase of power shortages after the turning point.

Figures 10b and 11b and Figs. 10c and 11c present the heat-electricity ratio and gas inertia output considering and not considering the gas network, respectively. It can be seen that there are also turning points on both the

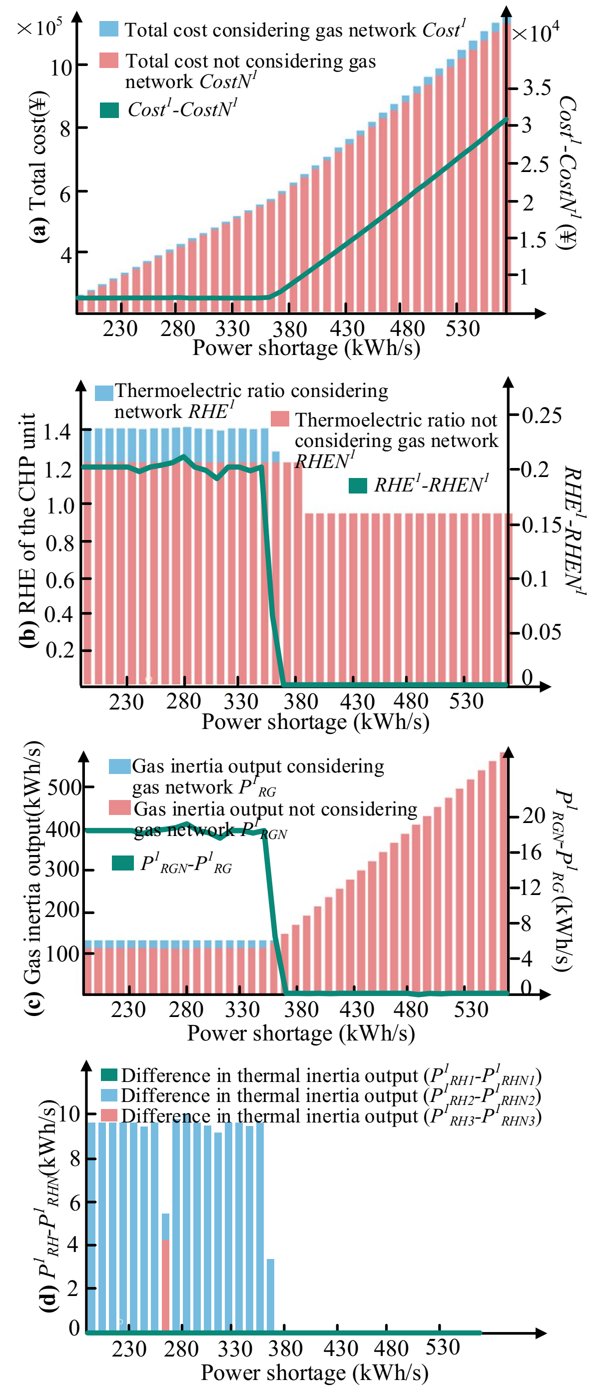

Fig. 10 Comparison results with power shortages at L_1

heat-electricity ratio difference curve and the gas inertia output difference curve. There are fluctuating differences between considering and not considering the gas network in the heat-electricity ratio and gas inertia output before the turning point. These drop to zero after the turning point regardless of the size of the power shortages.

Table 8 Comparisons of the total costs between considering gas network constraints *Cost* and not considering gas network constraints *CostN*

Power shortage (kWh/s)	*Cost* (¥)	*CostN* (¥)	*Cost–CostN* (¥)
(a) L_1			
200	274,260	267,250	7010
250	360,370	353,360	7010
300	446,470	439,470	7000
350	532,580	525,570	7010
400	653,430	642,360	11,070
450	787,130	770,520	16,610
500	922,780	900,400	22,380
(b) L_2			
200	274,920	267,250	7670
250	361,030	353,360	7670
300	447,130	439,470	7660
350	533,240	525,570	7670
400	654,120	642,360	11,760
450	787,350	770,520	16,830
500	921,940	900,400	21,540
(c) L_3			
300	445,230	439,470	5760
350	531,330	525,570	5760
400	650,800	642,360	8440
450	782,160	770,520	11,640
500	914,670	900,400	14,270
550	1,050,200	1,034,000	16,200

Figures 10d and 11d show the thermal inertia output differences from three load groups. Except for the thermal inertia output from the power shortage spot, which does not differ between considering and not considering the gas network, other thermal inertia output differences all drop to zero after the turning point.

It is worth noting that all the turning points are at the same power shortage size of 370 (kWh/s), which is not a coincidence. By observing each power output size and total cost before and after the turning point, the phenomenon can be explained as follows:

1. The unit cost of thermal inertia is lower than that of gas inertia. Assuming that user comfort is not significantly affected, the optimization model of power support will always prefer the use of thermal inertia output until it reaches the upper limit.
2. Before the turning point, the power shortage size is not very large, and the thermal inertia can respond to power shortages with gas inertia output without reaching its upper limit. In this way, the optimization model considering the gas network is not constrained

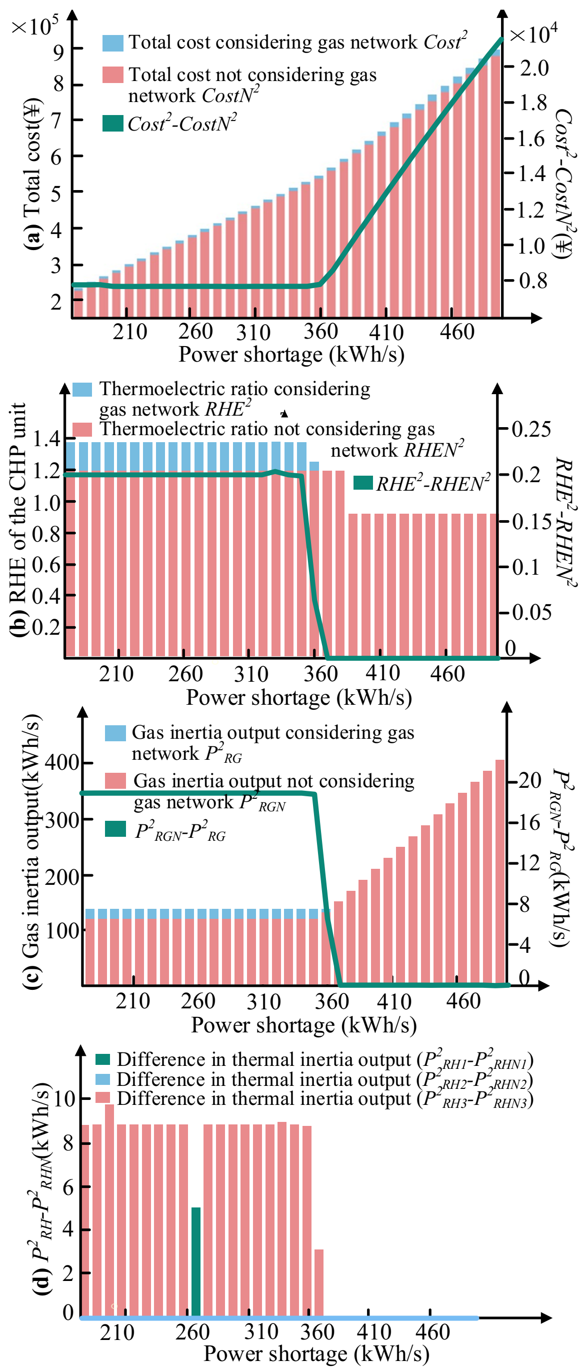

Fig. 11 Comparison results with power shortages at L_2

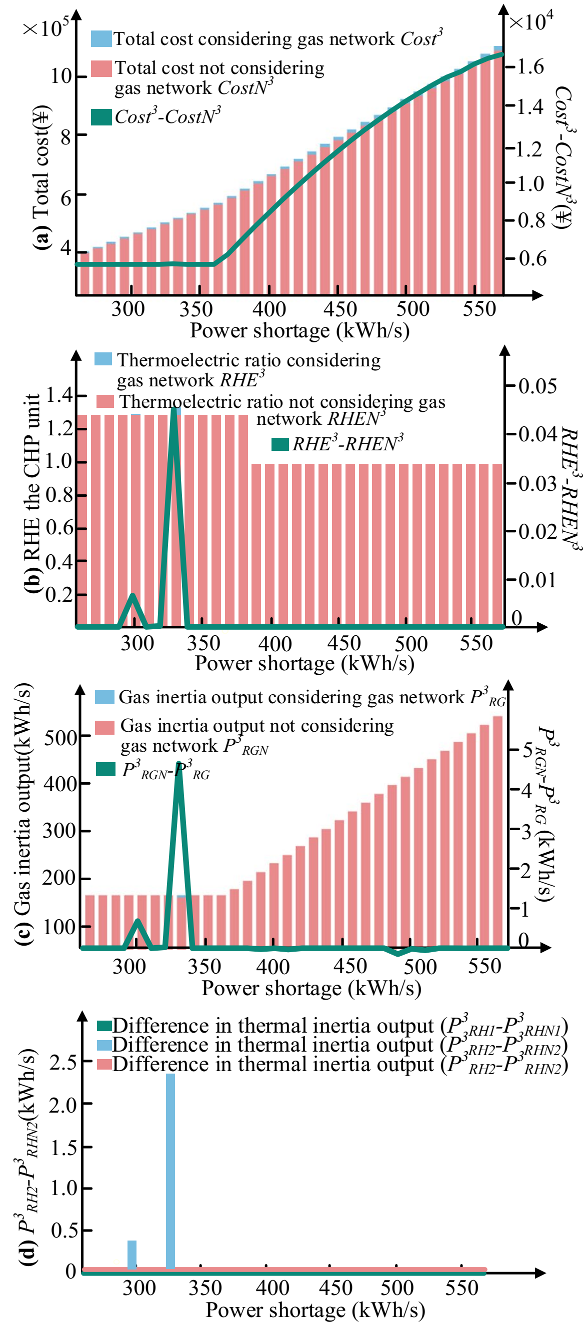

Fig. 12 Comparison results with power shortages at L_3

by the upper limit of thermal inertia, and can always flexibly use more thermal inertia output to avoid the higher cost of gas inertia, since the biggest difference between considering and not considering the gas network is the higher unit cost of gas inertia. Therefore, outputs when considering and not considering the gas network are different under different power shortages but the extra total costs remain the same.

3. After the turning point, both the outputs of thermal inertia considering and not considering the gas network reach the upper limits and the optimization flexibility is constrained. Therefore, with the increase of power shortages, the output of gas inertia will definitely increase and the difference of the total

cost when considering and not considering the gas network will also increase, given the higher unit cost of gas inertia considering the gas network under the same gas inertia output.

Considering the gas network can improve the power support model. The differences in the total cost, heat-electricity ratio, and gas-thermal inertia output in the comparison results also verify the research significance. However, based on the above-mentioned same turning point at different power shortage spots, it can also be concluded that in some conditions the network can be simplified if only a rough estimate is to be made in practical engineering application. In the case studied in Sect. 4.2, the turning point is the power shortage size of 370 (kWh/s). Solving the optimization model without considering the gas network can directly obtain the heat-electricity ratio and gas-thermal inertia output when the actual power shortages are larger than 370 (kWh/s). In contrast, the total cost without considering the gas network has the smallest deviation from the total cost considering the gas network when the actual power shortages are smaller than 370 (kWh/s). The advantages of the estimate without considering the network influence include easier modelling and faster computing speed, which are especially crucial to the strategy response speed. The computing speeds of the models with and without considering the gas network are 0.49 s and 0.07 s, respectively. However, the scales of actual engineering projects are much larger than the 8-node gas network used in the paper, so the differences in computing speed and modelling complexity will be further widened, and thus the importance of simplifying the gas network is further increased.

As for the power shortages at L_3 in Fig. 12, the turning point of the total cost difference is still 370 (kWh/s), but the turning points of the other three outputs are smaller while the overall differences in the three outputs have all decreased. This phenomenon does not affect the above conclusion obtained by setting the turning point as 370 (kWh/s), but it does indicate that the impact of the network is reduced when the power shortages are at L_3. Therefore, it is worth studying whether power shortage spots in the gas network can affect the power support results.

4.3 Analysis of the influence of power shortage spots

The respective differences in total cost, heat-electricity ratio and gas-thermal inertia output with and without considering the network influence during the power shortages at L_{1-3} are shown in Fig. 13.

Generally, the four differences with power shortages at L_{1-2} are close in size while the four differences with power shortages at L_3 are especially small. To analyse this phenomenon, all pipelines can be divided into 2 groups, with those in group 1 directly connected to the load and group 2 the remaining pipes in the gas network. Therefore, PL_{12} and PL_{23} are in group 1 when the power shortages are at L_1, PL_{34} is in group 1 when the power shortages are at L_2, while PL_{67} is in group 1 when the power shortages are at L_3. According to Figs. 7, 8 and 9, pipelines in group 1, given their direct connection to the load when power shortages occur, contribute more gas storage than those in group 2. However, there is only a small difference in the contribution of gas storage between the pipelines in group 1 and 2 when the power shortages are at L_{1-2}, but a great difference when the power shortages are at L_3. In other words, the contribution of gas storage is largely evenly-distributed to all the pipelines when the power shortages are at L_{1-2}, but mostly distributed to pipelines in group 1 when the power shortages are at L_3. The unit cost of gas storage in pipelines of group 1 is the same as that of gas storage without considering the gas network, which explains the reason why the four differences with the power shortages at L_3 are not so large in comparison with L_{1-2}.

As for the reason of the low gas network impact on L_3, it may be due to the fact that the load is at the downstream of the entire natural gas network and will not further affect the downstream gas storage because of the decrease in pressure caused by power shortage support. Although L_2 is also connected to the end of the pipe PL_{34}, it is not really the downstream load given that the gas flow in PL_{36} is from node 3 to node 6, which to some degree constrains the gas storage consumption in PL_{34}. Therefore, the power shortage spots can also be used as the basis to determine whether the network influence can be ignored. However, the 8-node gas network studied in this paper only consists of three

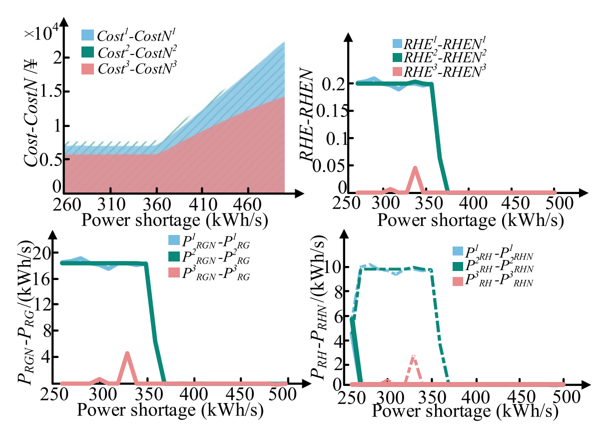

Fig. 13 Comparisons of the four differences with power shortages at L_{1-3}

load groups and the analysis of power shortage spots influence is inexhaustive. At the next stage, the power support model will be further refined based on the gas network with more load groups so that more data can be obtained for analysis. However, an improved well-grounded basis, which considers the power shortage spots influence to decide when the gas network influence can be ignored, has yet to be discovered.

4.4 Analysis of the influence factor of the power shortage turning point

The power shortage turning point of 370 (kWh/s) mentioned in Sect. 4.2 has been proved to provide the basis for the rough estimate of the system operational condition without considering network influence. The rough estimate is practical in the prediction of the total cost/power output and the improvement of the strategy response speed in engineering application. Typically, this specific turning point cannot be directly obtained from the basic parameters of IESs, which are necessary for the in-depth study of the influence factor of the power shortage turning point.

Based on the analysis in Sect. 4.2, it is found that the influence factor of the power shortage turning point is mainly the upper limit of the thermal inertia output, which can be directly obtained as the parameters of the IES itself. Therefore, the power shortage turning points S_P under different upper limits U_L of thermal inertia output are shown in Fig. 14 with a fitted curve of the relationship between S_P and U_L. The curve appears as the form of a linear function, which provides an approach to obtain U_L when S_P of the IES is known.

In order to illustrate the linear relationship between S_P and U_L, the specific relationships of thermal inertia output and power shortage size under five different upper limits of thermal inertia output are given in Fig. 14. Since the thermal inertia output comes from three different load groups, this section only chooses thermal inertia output from one load with higher unit output cost to study while the same is true for the other two loads. Before reaching the upper limit, the thermal inertia output increases proportionally with the increase of power shortages and remains unchanged after reaching the upper limit, which is exactly the time of the flexibility of thermal inertia output being constrained and the appearance of the power shortage turning point. With the regular increase of the upper limit of thermal inertia output, the corresponding curve will also shift to the upright proportionally. Therefore, the five curves can be expressed before reaching the upper limit of thermal inertia output, as:

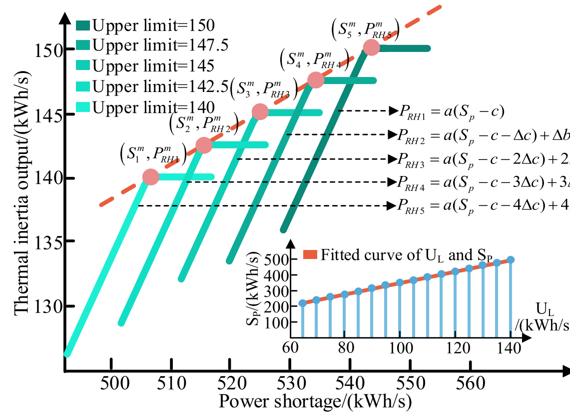

Fig. 14 The curve of S_P-U_L and relative illustration curves under different upper limits of thermal inertia output

$$\begin{cases} P_{RH1} = a(S_p - c) \\ P_{RH2} = a(S_p - c - \Delta c) + \Delta b \\ P_{RH3} = a(S_p - c - 2\Delta c) + 2\Delta b \\ P_{RH4} = a(S_p - c - 3\Delta c) + 3\Delta b \\ P_{RH5} = a(S_p - c - 4\Delta c) + 4\Delta b \end{cases} \tag{28}$$

The five turning points (S_1^m, P_{RH1}^m), (S_2^m, P_{RH2}^m), (S_3^m, P_{RH3}^m), (S_4^m, P_{RH4}^m), and (S_5^m, P_{RH5}^m) fit in each of these five formulas:

$$\begin{cases} P_{RH1}^m = a(S_1^m - c) \\ P_{RH2}^m = a(S_2^m - c - \Delta c) + \Delta b \\ P_{RH3}^m = a(S_3^m - c - 2\Delta c) + 2\Delta b \\ P_{RH4}^m = a(S_4^m - c - 3\Delta c) + 3\Delta b \\ P_{RH5}^m = a(S_5^m - c - 4\Delta c) + 4\Delta b \end{cases} \tag{29}$$

The slopes of the lines formed between these five points are found to be the same, which can prove that these five points are on the same line and the slope is given in (30). These 5 points are just 5 special cases on the curve of the relationship between S_P and U_L, but the illustration of these 5 points is enough to explain the forming reason of the linear S_P-U_L curve.

$$\begin{aligned} k_{P-S} &= \frac{P_{RH2}^m - P_{RH1}^m}{S_2^m - S_1^m} = \frac{P_{RH3}^m - P_{RH2}^m}{S_3^m - S_2^m} \\ &= \frac{P_{RH4}^m - P_{RH3}^m}{S_4^m - S_3^m} = \frac{P_{RH5}^m - P_{RH5}^m}{S_4^m - S_4^m} \\ &= \frac{\Delta b}{\Delta c} \end{aligned} \tag{30}$$

The fitted curve in Fig. 14 has application value in real projects. When the upper limit of the thermal inertia output in an IES is known, the actual size of power shortages can be compared with the power shortage turning point to decide whether the gas network constraints can be simplified and which parameters can be roughly estimated.

1. If the actual power shortages are larger than the power shortage turning point, the heat-electricity ratio and gas-thermal inertia output can be directly estimated without considering the gas network.
2. If the actual power shortages are smaller than the power shortage turning point, the total cost without considering the gas network has the smallest deviation from that considering the gas network.

Therefore, the curve of S_P-U_L can guide IES power output schemes in engineering practice. Since the upper limit of thermal inertia output is usually the known parameter of IESs, the power output scheme and the strategy economy can be estimated and evaluated before actual power support takes place.

5 Conclusion

In this paper, the definition and modelling of gas inertia in integrated energy systems are described. A multi-energy inertia-based power support strategy considering the gas network constraints is proposed with its effectiveness verified in an actual scenario. The following conclusions can be drawn:

1. Gas inertia can provide buffer space to accommodate power fluctuations. This provides the foundation for gas-thermal inertia utilization in the power support strategy.
2. The significance of considering gas network constraints is verified through the comparisons of results of not considering gas network constraints. By consideration of the gas network, the optimization model accuracy for total cost has been improved by about 1.8–3.0%.
3. Despite the gas network influence on the power support results, it can still be simplified under certain circumstances to obtain a rough estimate of the power support condition. The prediction error of the total cost after simplification is about 2.8%, and the prediction error of heat-electricity ratio, gas-thermal inertia outputs after simplification is about 0.1%. Gas network simplification can reduce modelling complexity and increase the computing speed by about 34% for the improvement of the response speed of the power support strategy.

In future research, the multi-energy inertia-based power support model will be further refined based on a more specific natural gas network model considering the gas compressor modelling or more connected load groups. The current relatively conservative integrated energy system power support scheme can be improved for expanded application in a more practical complex system.

Acknowledgements
Not applicable.

Author contributions
CM: Methodology, Data curation, Investigation, Writing-Original draft preparation. QW: Conceptualization, Methodology, Supervision, Reviewing. YT: Supervision. All authors read and approved the final manuscript.

Funding
This work was supported by National Key R&D Program of China (No. 2019YFE0118000).

Availability of data and materials
The datasets used and/or analyzed during the current study are available from the corresponding author on reasonable request.

Declarations

Competing interests
The authors declare that they have no known competing financial interests or personal relationships that could have appeared to influence the work reported in this paper.

Received: 14 November 2022 Accepted: 11 April 2023
Published online: 19 April 2023

References

1. Strunck, C., Albrecht, M., Rehtanz, C., et al. (2019). Provision of ancillary service by different decentralized energy resources. In *2019 IEEE Milan PowerTech*.
2. Tang, Y., Li, F., Chen, Q., et al. (2018). Frequency prediction method considering demand response aggregate characteristics and control effects. *Applied energy, 229*, 936–944.
3. Cui, Y., Song, P., Wang, X., et al. (2018). Wind power virtual synchronous generator frequency regulation characteristics. In *2018 2nd International conference on green energy and applications (ICGEA)* (pp. 193–196).
4. Chen, J., Yang, R., Xu, D., et al. (2021). Maximum production point tracking method for a solar-boosted biogas energy generation system. *Protection and Control of Modern Power Systems, V6*(4), 525–537.
5. Liu, S., Zhou, C., Guo, H., et al. (2021). Operational optimization of a building-level integrated energy system considering additional potential benefits of energy storage. *Protection and Control of Modern Power Systems, V6*(1), 55–64.
6. Huang, Z., Fang, B., & Deng, J. (2020). Multi-objective optimization strategy for distribution network considering V2Genabledelectric vehicles in building integrated energy system. *Protection and Control of Modern Power Systems, V5*(1), 48–55.
7. Wang, R., Cheng, S., Zuo, X., & Liu, Y. (2022). Optimal management of multi stakeholder integrated energy system considering dual incentive demand response and carbon trading mechanism. *International Journal of Energy Research, 46*, 6246–6263.
8. Saedi, I., Mhanna, S., & Mancarella, P. (2021). Integrated electricity and gas system modelling with hydrogen injections and gas composition tracking. *Applied Energy, 303*, 117598.
9. Xu, X., Ming, W., Zhou, Y., & Wu, J. (2019). Coordinative control of CHP generation and battery for frequency response. In *2019 IEEE power & energy society general meeting (PESGM)*. IEEE.

10. Trifonov, T. (2017). Coordination of battery energy storage and power-to-gas in distribution systems. *Protection and Control of Modern Power Systems, V2*(4), 421–428.
11. Li, X., Li, W., Zhang, R., Jiang, T., Chen, H., & Li, G. (2020). Collaborative scheduling and flexibility assessment of integrated electricity and district heating systems utilizing thermal inertia of district heating network and aggregated buildings. *Applied Energy, 258*, 114021.
12. Yang, X., Chen, Z., Huang, X., et al. (2021). Robust capacity optimization methods for integrated energy systems considering demand response and thermal comfort. *Energy, 221*, 119727.
13. Sesini, M., Giarola, S., & Hawkes, A. D. (2021). Strategic natural gas storage coordination among EU member states in response to disruption in the trans Austria gas pipeline: A stochastic approach to solidarity. *Energy, 235*, 121426.
14. Yu, W., Gong, J., Song, S., et al. (2019). Gas supply reliability analysis of a natural gas pipeline system considering the effects of underground gas storages. *Applied Energy, 252*, 113418.
15. Ordoudis, A., Pinson, P., & Morales, J. (2019). An integrated market for electricity and natural gas systems with stochastic power producers. *European Journal of Operational Research, 272*(1), 642–654.
16. Fan, J., Tong, X., & Zhao, J. (2020). Multi-period optimal energy flow for electricity-gas integrated systems considering gas inertia and wind power uncertainties. *Electrical Power and Energy Systems, 123*, 106263.
17. Wang, Q., Miao, C., & Tang, Y. Power shortage support strategies considering unified gas-thermal inertia in an integrated energy system. *Applied Energy*. Accepted.
18. Miao, C., Wang, Q., & Tang, Y. A gas-thermal inertia-based frequency response strategy considering the suppression of a second frequency dip in an integrated energy system. *Energy*. Accepted.
19. Sun, W., Wang, Q., Ye, Y., et al. (2022). Unified modelling of gas and thermal inertia for integrated energy system and its application to multitype reserve procurement. *Applied Energy, 305*, 117963.
20. Zhu, M., Xu, C., Dong, S., et al. (2021). An integrated multi-energy flow calculation method for electricity-gas-thermal integrated energy systems. *Protection and Control of Modern Power Systems, V6*(1), 65–76.
21. Correa-Posada, C. M., & Pedro, S. (2015). Integrated power and natural gas model for energy adequacy in short-term operation. *IEEE Transactions of power system, 30*(6), 3347–3355.
22. Qiao, Z., Guo, Q., Sun, H., & Sheng, T. (2018). Multi-time period optimized configuration and scheduling of gas storage in gas-fired power plants. *Applied Energy, 226*, 924–934.
23. Junesoo, S., Yannick, W., & Jalal, K. (2022). Modeling gas flow directions as state variables: Does it provide more flexibility to power systems? *Electric Power Systems Research, 212*, 108502.
24. Tomasson, E., & Soder, L. (2020). Coordinated optimal strategic demand reserve procurement in multi-area power systems. *Applied Energy, 270*, 1–10.